

Supporting Information: Structure Sensitivity in Pt-Catalyzed Hydrodeoxygenation of Multi-Oxygenated Lignin Model Compounds

Justin Marlowe^a, Mahdi Abu-Omar^{a,b}, Phillip Christopher^a

^aDepartment of Chemical Engineering, University of California, Santa Barbara, Santa Barbara, CA
93106, United States

^bDepartment of Chemistry and Biochemistry, University of California, Santa Barbara, Santa Barbara, CA
93106, United States

Table of Contents:

Figure S1: Surface Site Fractions of Model Cuboctahedron Geometries

Figure S2: Additional HAADF-STEM Images of 0.4-Pt

Figure S3: HAADF-STEM Images of 2.0-Pt

Figure S4: Additional HAADF-STEM Images of 6.0-Pt

Figure S5: 6.0-Pt Particle Size Distributions from HAADF-STEM

Figure S6: Volume-Normalized Particle Size Distribution for 0.4-Pt

Figure S7: Details and Examples of Gaussian Peak Deconvolution for CO DRIFTS

Figure S8: CO DRIFTS Peak Shape of 6.0-Pt in Absorbance vs. Kubelka-Munk Units

Figure S9: DRIFTS Spectrum of Spent 0.4-Pt After 2-Hour DHE HDO Reaction

Figure S10: Gas Chromatogram of Head Space After Reaction

Figure S11: Pressure Dependent Studies of DHE HDO over 6.0-Pt

Figure S12: Full Time Profiles of DHE HDO over 0.4-Pt and 6.0-Pt

Table S1: Tabulation of Isoconversion DHE Reaction Results (Figure 2)

Table S2: Tabulation of Time Profile Experiments (Figure 4)

Table S3: Tabulation of Pressure Variation Experiments (Figure 5)

Table S4: Tabulation of Isoconversion PHE Reactions (Figure 6)

Table S5: Full Mass Balance Closure of DHE Isoconversion Experiments

S.I. Note 1: Estimation of Reaction Equilibrium for Aromatic Oxygenates in the Liquid Phase**

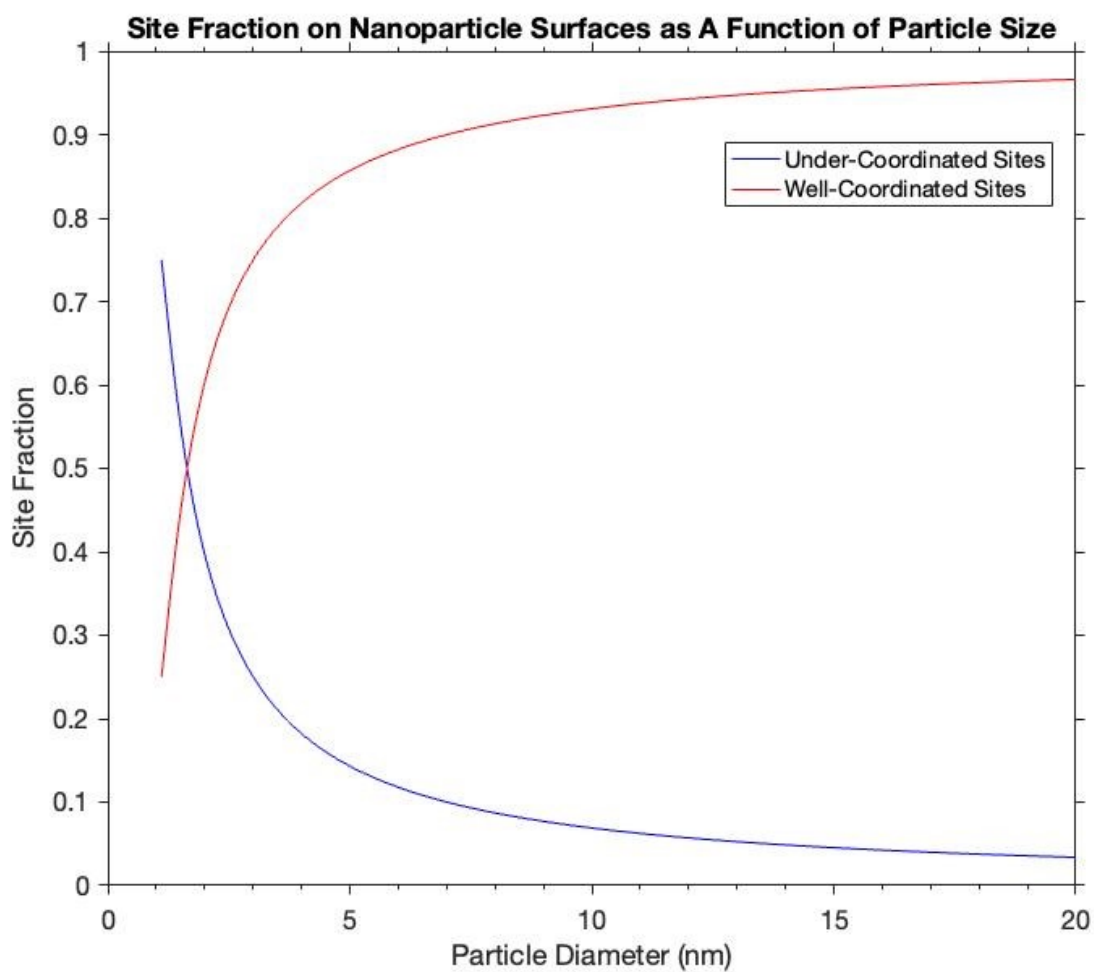


Figure S1: Fraction of well-coordinated and under-coordinated sites on the surface of metal nanoparticles as a function of particle diameter. In conjunction with CO DRIFTS spectral deconvolution, this model enables estimation of metal particle size directly from CO DRIFTS experiments.

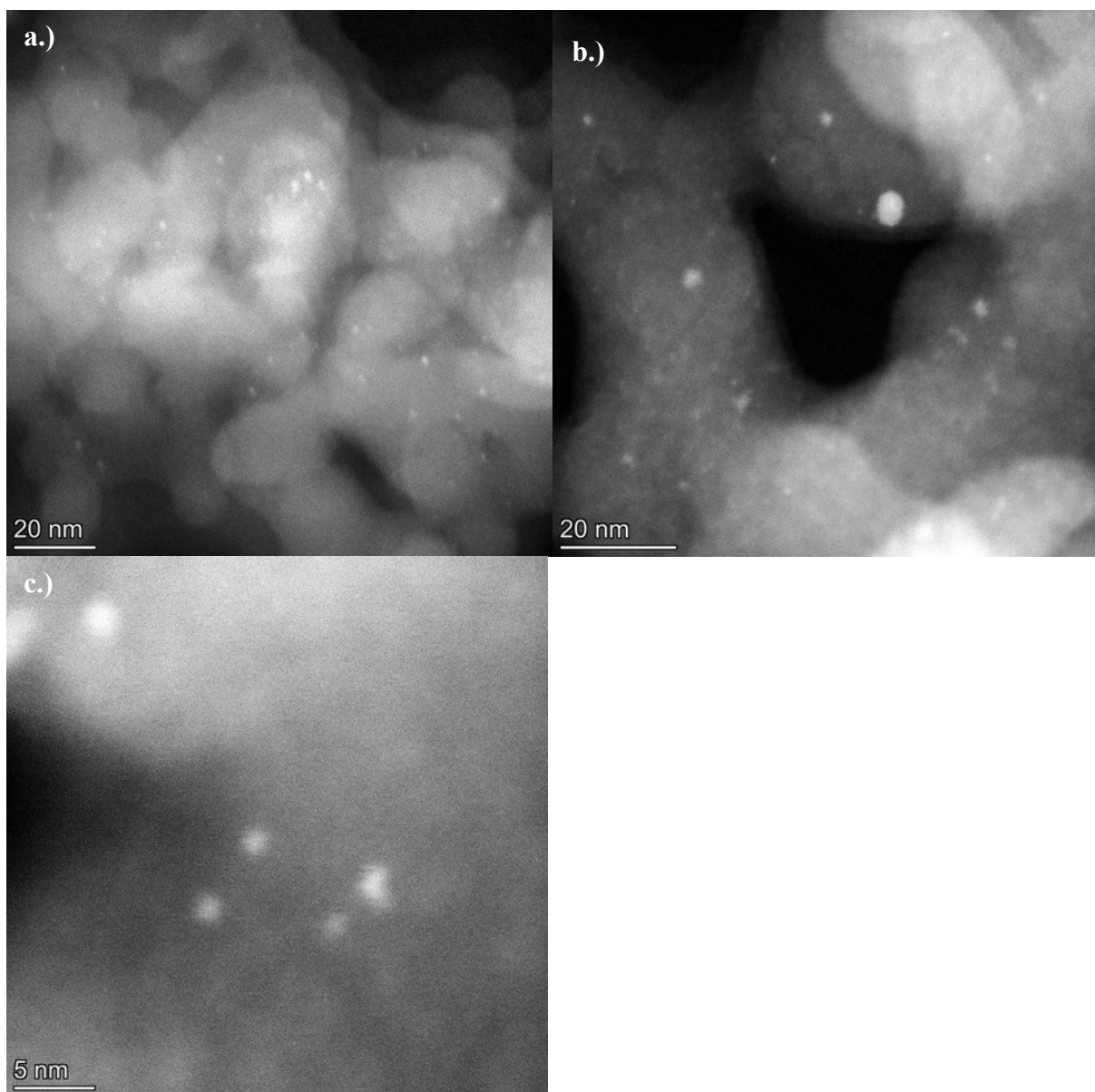


Figure S2: a-c.) Additional HAADF-STEM images of 0.4-Pt. c.) shows an example of approximately 1 nm Pt clusters which were present across the sample.

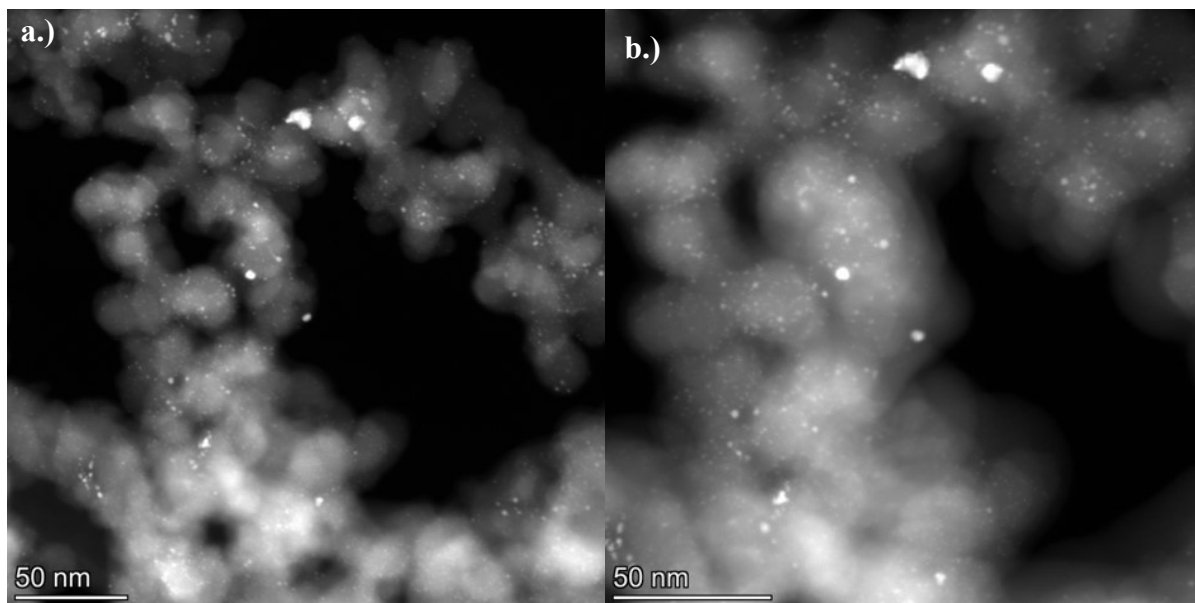


Figure S3: a-b.) HAADF-STEM images of 2.0-Pt.

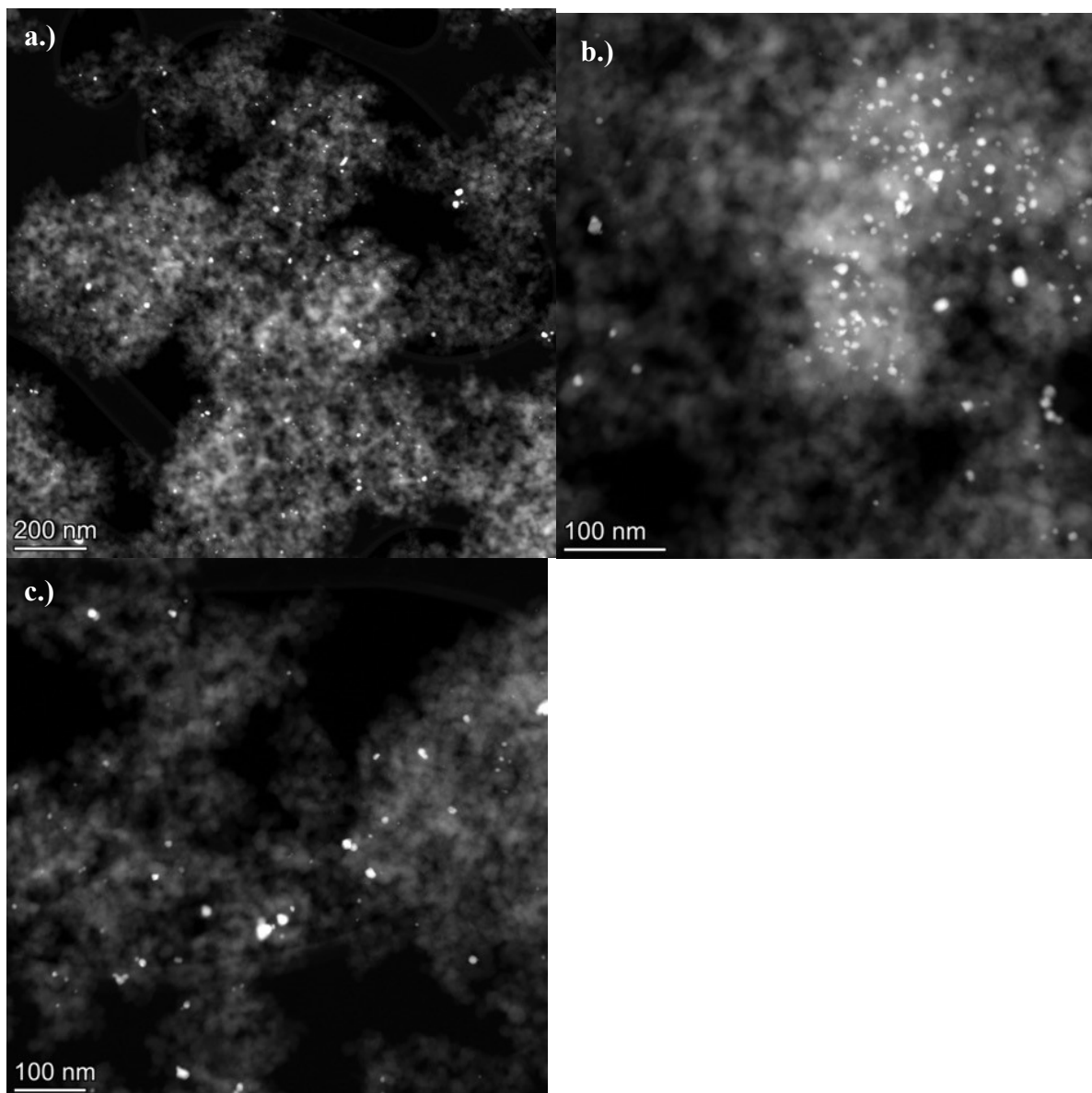


Figure S4: a-c.) HAADF-STEM images of 6.0-Pt. Low-magnification images highlight the presence of significantly larger Pt particles than on other samples.

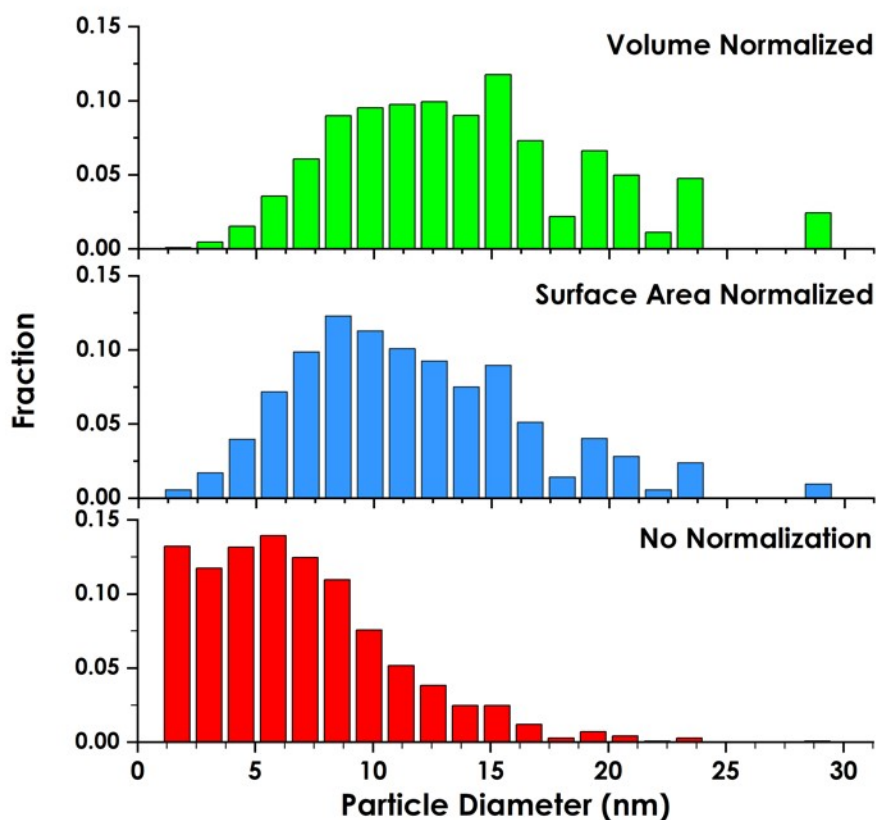


Figure S5: Particle size distributions obtained for 6.0-Pt represented by different data presentations. Surface-normalization is preferred for the discussion of reactivity since this provides a representative presentation of metal surface area in the sample, which is the active site for reactivity. In contrast, volume-normalization over-estimates the average particle size because of the weighting of large nanoparticles, despite their limited contribution to the total catalytically active metal surface area.

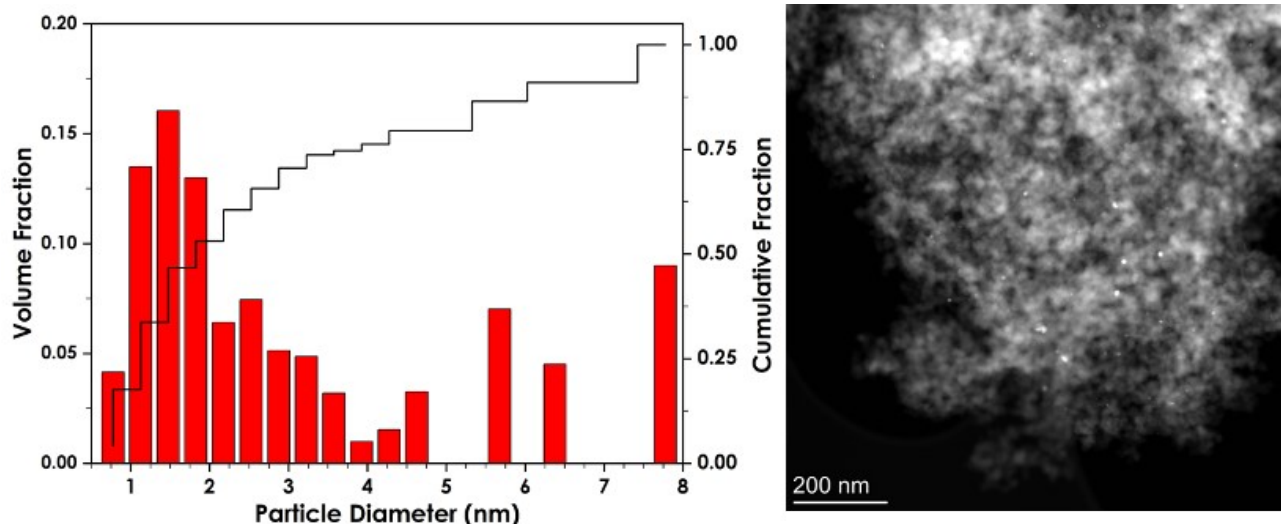


Figure S6: Results from CO chemisorption to estimate Pt dispersion gave consistently lower values from those expected from either HAADF-STEM images or CO-DRIFTS experiments, particularly for 0.4% Pt catalysts. Collection of a large number of STEM images for 0.4-Pt allowed the identification of a small number of unexpectedly large nanoparticles (>5 nm), even for this small loading of Pt on relatively high surface area silica. Incorporation of these outlier nanoparticles into the particle size distribution of the over 1000 particles analyzed does not immediately resolve the CO chemisorption results. However, consideration of the volume-normalized particle size distribution, where the contribution of each particle to the total imaged Pt volume is plotted, clearly demonstrates that these outlier nanoparticles contain a sizeable fraction of the total Pt. Due to the decrease in surface area to volume ratio with particle size, though, most of this Pt is not available for CO adsorption. Thus, these outlier particles significantly alter the standard estimates of particle size by CO chemisorption-measured dispersion, resulting in the differences in particle size estimation techniques for 0.4-Pt.

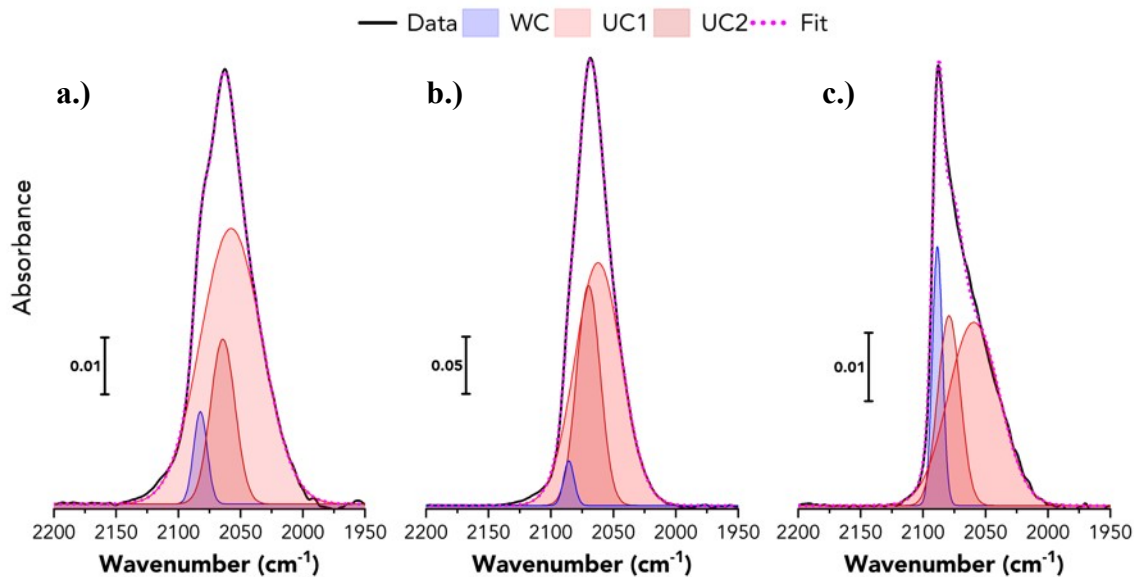


Figure S7: Spectral deconvolution of CO DRIFTS spectra shown in Figure 2c. Deconvolution uses 3 Gaussian features to best represent the experimentally obtained spectra, with specifically 2 Gaussian features (UC1 and UC2) used to describe the UC site peak shape, which has been frequently observed to be asymmetric. For fitting, peak maxima and intensity were set as free parameters, while peak FWHM was constrained between the same limits for all catalysts. Allowing peak maxima to change freely captures the changing spectral signature of geometrically identical CO features with increasing dipole-dipole coupling, most noticeably observed for CO linearly bound to WC Pt terraces. Increased dipole-dipole coupling with increasing terrace size (and Pt particle size) results in a blue-shift and narrowing of the feature, despite the peak corresponding to the same structural motif (i.e. WC sites).

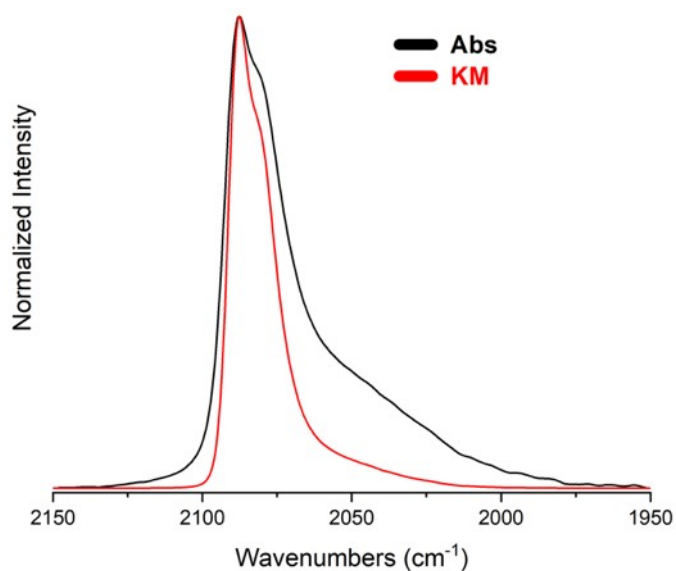


Figure S8: 6.0-Pt CO DRIFTS spectrum represented in both Absorbance and Kubelka-Munk units. Spectra have been normalized to the maximum peak height to demonstrate the changes in peak shape and width that complicate particle size estimation. Kubelka-Munk representation tends to exaggerate DRIFTS features of stronger intensity, resulting in a narrowing of the overall CO feature. This then changes the relative areas of WC- and UC-bound CO features, which is the measure used to related CO DRIFTS to model geometries. Considering the open use of both units in CO DRIFTS in literature, we opt to use a range of particle sizes from both Absorbance and Kubelka-Munk fits in our particle size estimation approach.

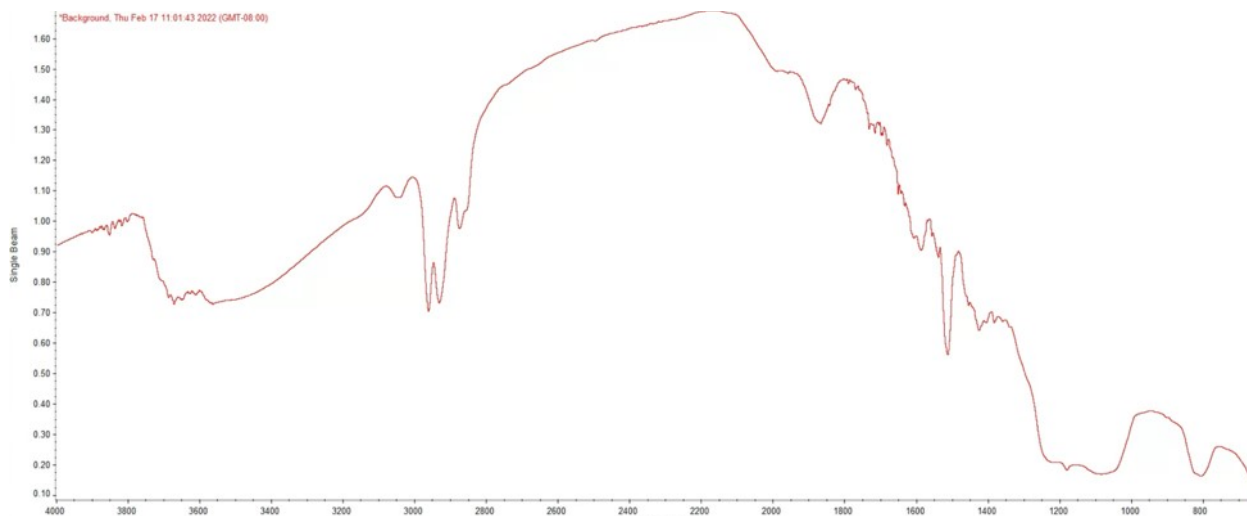


Figure S9: DRIFTS spectrum of a spent 0.4-Pt catalyst after 2 hour DHE isoconversion reaction. Peak features include strong C-H stretches (2800-3000 cm^{-1}), C=C stretches (1550 cm^{-1}), and C-O stretches (1225 cm^{-1}) which point to the strong adsorption of reaction intermediates on the catalyst surface. Importantly, the presence of C-O stretching is indicative of adsorbed oxygenates such as oligomers formed during reaction as opposed to coking on the catalyst surface, which would exhibit weaker, if any, C-H and C-O stretching features.

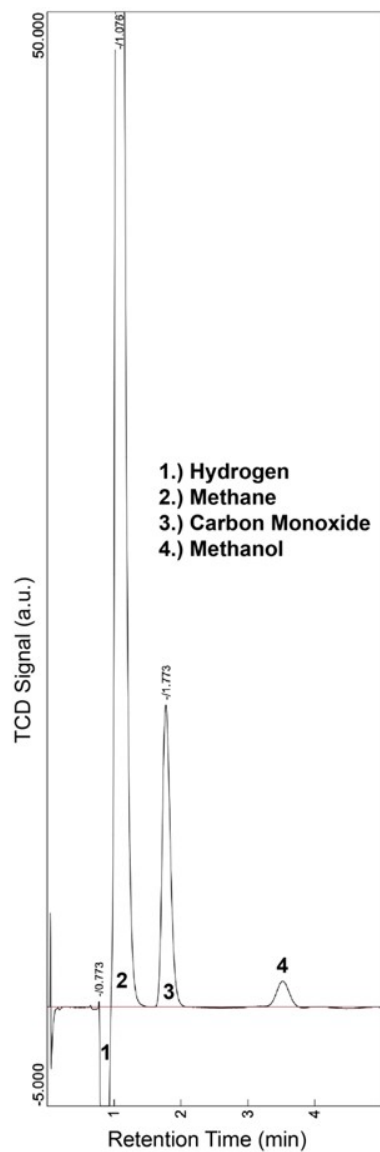


Figure S10: TCD-measured gas chromatogram of the head space after a typical DHE HDO reaction over 6.0-Pt. The species identified are most likely produced from the demethoxylation and demethylation of DHE, directly forming methanol and CH_4 , respectively. CO is produced from the decomposition of methanol to CO and H_2 . The absence of features corresponding to light alkanes (C_2^+) is evidence for the lack of cracking reactions, either of substrates, products, or solvent.

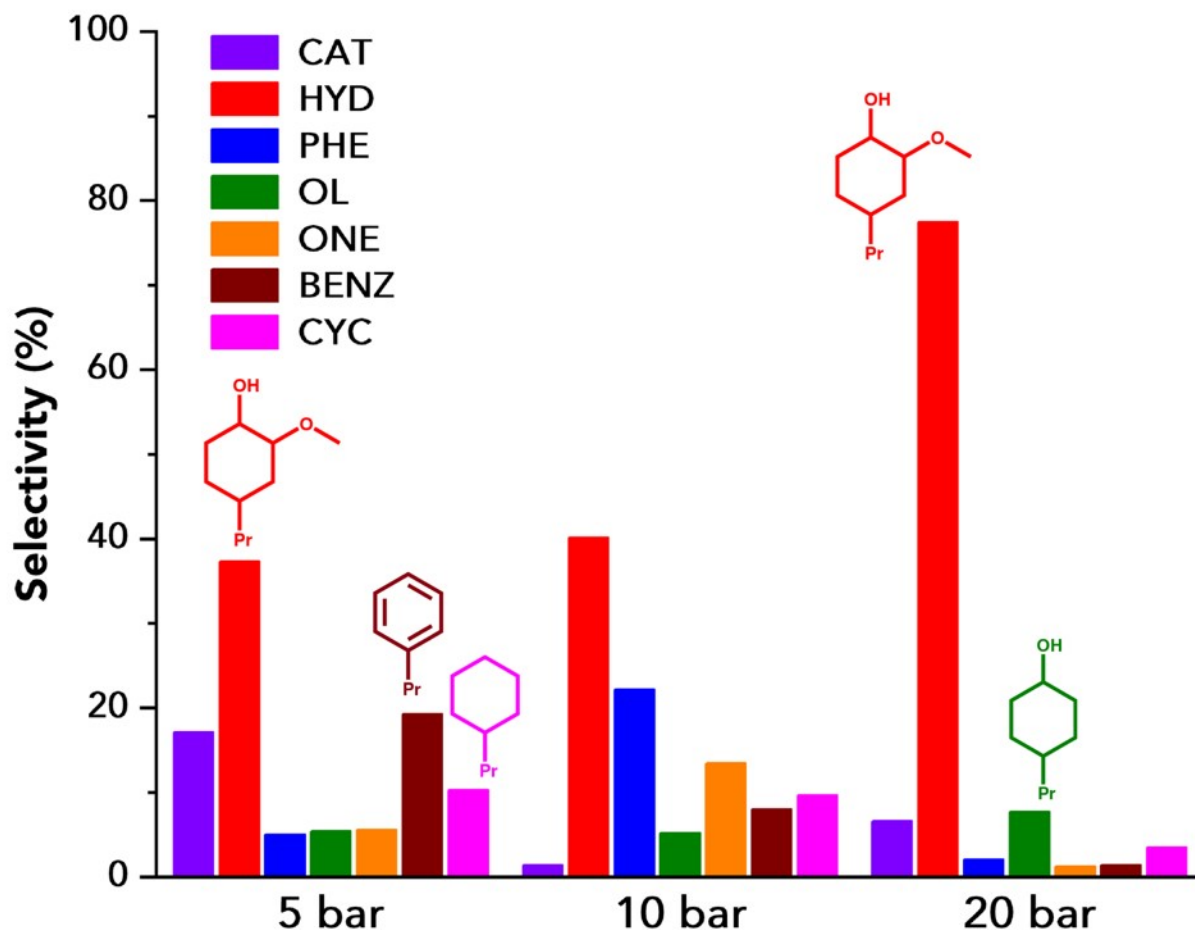


Figure S11: Pressure-dependent HDO reactions of DHE over 6.0-Pt. Isoconversion of ~30% was obtained by altering the catalyst loading. *Conditions:* 275°C, 2 hours, 500 mg DHE, 20 mL cyclohexane. For all pressures studied, HYD is the dominant product, in line with the observation of favored aromatic ring hydrogenation over 6.0-Pt in all other experiments conducted. Additionally, BENZ and CYC are formed in significant quantities at all pressures, in stark contrast to the 0.4-Pt catalyst which does not yield fully deoxygenated species, regardless of H₂ pressure. BENZ and CYC selectivity drops with increasing H₂ pressure, likely due to the increasing selectivity to HYD. As discussed in the main text, HYD is considered a dead end intermediate due to the inactivity of saturated ring species in the HDO pathway over non-acidic catalyst.

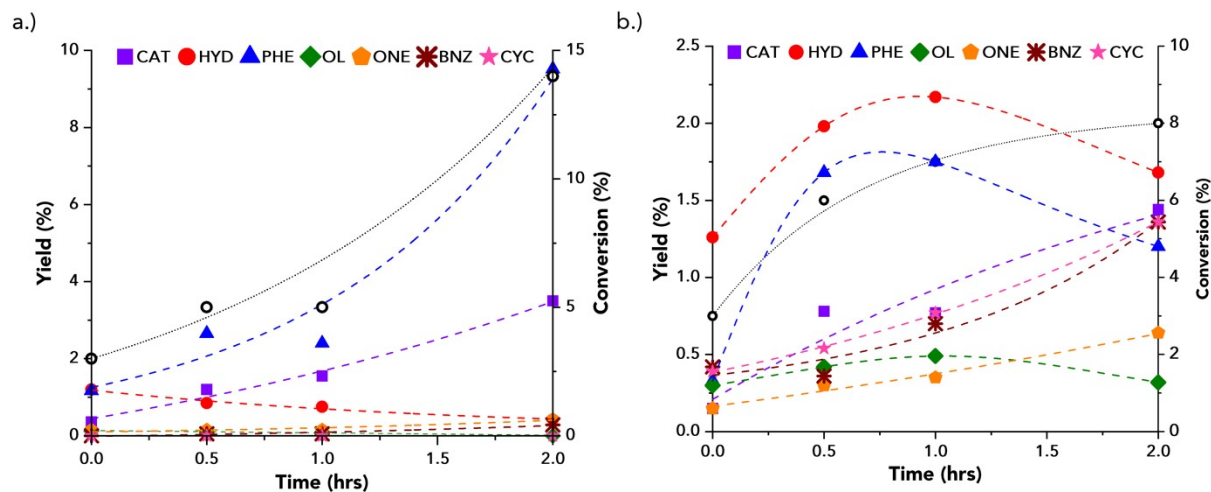


Figure S12: Full time profile reactivity for DHE HDO over a.) 0.4-Pt and b.) 6.0-Pt. As pointed out in the main text, CAT yield increases monotonically in time regardless of PHE behavior over both catalysts, indicating that PHE is not a direct product of CAT dehydroxylation.

| Catalyst | Catalyst Loading (mg) | Conversion (%) | Mass Balance (%) | Yield (%) | Selectivity (%) | | | | | | |
|----------|-----------------------|----------------|------------------|-----------|-----------------|-----|-----|----|-----|-----|-----|
| | | | | | CAT | HYD | PHE | OL | ONE | BNZ | CYC |
| 0.4-Pt | 50 | 15 | 88 | 2 | 25 | 3 | 67 | 0 | 3 | 2 | 0 |
| 2.0-Pt | 15 | 15 | 89 | 4 | 15 | 25 | 53 | 4 | 2 | 0.5 | 0 |
| 6.0-Pt | 20 | 8 | 93 | 2 | 18 | 21 | 15 | 4 | 8 | 17 | 17 |

Table S1: Tabulated conversions, mass balances, yields, and selectivities for DHE HDO reactions over various Pt/SiO₂ catalysts. Isoconversion of ~15% was obtained by altering the catalyst loading as shown. *Conditions:* 275°C, 2 hours, 500 mg DHE, 20 mL cyclohexane, 10 bar H₂

| Time | Conversion (%) | Mass Balance (%) | Yield (%) | Selectivity (%) | | | | | | |
|------|----------------|------------------|-----------|-----------------|-----|-----|----|-----|-----|-----|
| | | | | CAT | HYD | PHE | OL | ONE | BNZ | CYC |
| 0 | 3 | 98 | 1 | 12 | 40 | 39 | 4 | 5 | 0 | 0 |
| 0.5 | 5 | 93 | 2 | 24 | 17 | 53 | 2 | 3 | 1 | 0 |
| 1 | 5 | 97 | 2 | 31 | 15 | 48 | 2 | 3 | 1 | 0 |
| 2 | 14 | 88 | 2 | 25 | 3 | 68 | 0 | 3 | 2 | 0 |

Table S2a: Tabulated conversions, mass balances, yields, and selectivities for the 0.4-Pt time profile reactions. Reactions conducted with 20 mg catalyst per reaction. *Conditions:* 275°C, 500 mg DHE, 50 mg catalyst, 20 mL cyclohexane, 10 bar H₂

| Time | Conversion (%) | Mass Balance (%) | Yield (%) | Selectivity (%) | | | | | | |
|------|----------------|------------------|-----------|-----------------|-----|-----|----|-----|-----|-----|
| | | | | CAT | HYD | PHE | OL | ONE | BNZ | CYC |
| 0 | 3 | 99 | 3 | 5 | 42 | 11 | 10 | 5 | 13 | 14 |
| 0.5 | 6 | 96 | 3 | 13 | 22 | 28 | 7 | 5 | 9 | 3 |
| 1 | 7 | 96 | 2 | 11 | 31 | 25 | 7 | 5 | 11 | 10 |
| 2 | 8 | 93 | 2 | 18 | 21 | 15 | 4 | 8 | 17 | 17 |

Table S2b: Tabulated conversions, mass balances, yields, and selectivities for the 6.0-Pt time profile reactions. Reactions conducted with 20 mg catalyst per reaction. *Conditions:* 275°C, 500 mg DHE, 20 mg catalyst, 20 mL cyclohexane, 10 bar H₂

| Pressure (bar) | Catalyst Loading (mg) | Conversion (%) | Mass Balance (%) | Yield (%) | Selectivity (%) | | | | | |
|----------------|-----------------------|----------------|------------------|-----------|-----------------|-----|----|-----|-----|-----|
| | | | | | HYD | PHE | OL | ONE | BNZ | CYC |
| 5 | 750 | 54 | 68 | 21 | 13 | 66 | 4 | 9 | 0 | 1 |
| 10 | 500 | 62 | 64 | 27 | 24 | 42 | 9 | 15 | 0 | 5 |
| 20 | 125 | 46 | 74 | 20 | 50 | 21 | 22 | 5 | 0 | 1 |

Table S3: Tabulated conversions, mass balances, yields, and selectivities for pressure-dependent HDO experiments using 0.4-Pt. Isoconversion of ~50% was obtained by altering the catalyst loading as shown. *Conditions:* 275°C, 2 hours, 500 mg DHE, 20 mL cyclohexane, 10 bar H₂

| Catalyst | Catalyst Loading (mg) | Conversion (%) | Mass Balance (%) | Yield (%) | Selectivity (%) | | | |
|----------|-----------------------|----------------|------------------|-----------|-----------------|-----|-----|-----|
| | | | | | OL | ONE | BNZ | CYC |
| 0.4-Pt | 50 | 25 | 91 | 17 | 51 | 35 | 12 | 2 |
| 2.0-Pt | 15 | 22 | 93 | 15 | 27 | 68 | 5 | 1 |
| 6.0-Pt | 16.5 | 25 | 95 | 20 | 16 | 35 | 45 | 4 |

Table S4: Tabulated conversions, mass balances, yields, and selectivities for PHE HDO reactions over various Pt/SiO₂ catalysts. Isoconversion of ~25% was obtained by altering the catalyst loading as shown. *Conditions:* 275°C, 2 hours, 500 mg PHE, 20 mL cyclohexane, 10 bar H₂

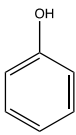
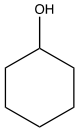
Table 2

| Sample | Adsorbed Organics |
|--------------------------|----------------------|
| | Weight Change (mg/g) |
| 0.4% Pt/SiO ₂ | 127.6 |
| 6% Pt/SiO ₂ | 206.4 |

Table S5: Quantification of adsorbed organics on catalyst surface after typical DHE HDO reactions. Catalysts were separated from the reaction mixture by centrifugation and kept under vacuum for 24 hours to evaporate all solvent. The dried catalyst was then weighed before calcination under air at 500°C for 2 hours to combust all adsorbed organic material. The mass loss after was recorded as shown above, corresponding to <5% of the mass balance for typical reactions. Combined with post-reaction DRIFTS shown in Figure S9, which indicates these species are likely oligomeric and not carbonaceous in nature, this points to the mass balance loss being primarily related to soluble oligomeric oxygenates not detectable by GC.

S.I. Note 1: Estimation of Reaction Equilibrium for Aromatic Oxygenates in the Liquid Phase

HDO reaction of DHE over 0.4-Pt catalysts at low and high conversions under 10 bar (gauge) of H₂ indicated that unsaturated aromatic compounds such as PHE and CAT were favored over the analogous saturated compounds (i.e. cyclohexanol, cyclohexanone, cyclohexa-1,2-diol). However, pressure studies demonstrated that the 0.4-Pt catalyst is capable of performing aromatic ring hydrogenation at reaction conditions. Thus, the preferential formation of unsaturated species over 0.4-Pt at under specific H₂ pressures, i.e. under 10 bar of H₂, is likely the result of equilibrium limitations on the extent of hydrogenation. To support this, the following estimates were made of the equilibrium position for a model reaction of phenol hydrogenation, which was chosen due to the availability of thermochemical data.

| Species | $\Delta H_{f,g}^0$ (kJ/mol) | $S_{f,g}^0$ (J/mol*K) |
|--|-----------------------------|-----------------------|
| H ₂ | 0 | 130 (Ref. [2]) |
|  | -91.8 (Ref. [4]) | 316 (Ref. [5]) |
|  | -290.8 (Ref. [1]) | 353.8 (Ref. [3]) |

Using these values, the standard changes in enthalpy and entropy of reaction can be calculated as:

$$\Delta H_{rxn}^0 = \sum v_i \Delta H_f^0$$

$$S_{rxn}^0 = \sum v_i S_f^0$$

Where v_i is the stoichiometric factor of the reaction. From this, the equilibrium constant can be estimated assuming that ΔH_{rxn}^0 and S_{rxn}^0 are temperature independent via:

$$\ln K = -\frac{\Delta H_{rxn}^0}{RT} + \frac{S_{rxn}^0}{R}$$

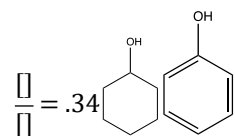
At 275°C, this gives a value of $K = 3.74$. This can be related to the composition of the reaction by representing the equilibrium constant as:

$$K = \frac{[\text{Cyclohexanol}]}{[\text{Phenol}] [\text{H}_2]^3}$$

In the case of liquid phase reactions, as conducted here, the concentration of H₂ is not immediately obvious. To capture the availability of hydrogen in the reaction medium (the liquid-catalyst interface), gas solubility data was interpolated for the conditions of interest (275°C, ~50 bar total pressure). This provided an estimated molar fraction of H₂ in the liquid phase of 0.047. This mole fraction can be represented as a molarity by:

$$[H_2] = \frac{x_{H_2,l} V_{M,Cyc}}{(1 - x_{H_2,l})}$$

Where $x_{H_2,l}$ is the mole fraction of H₂ in the liquid phase and V_M is the molar volume of cyclohexane, which is the overwhelmingly dominant component of the liquid phase as the solvent in mol/mL. This gives a H₂ molarity of 0.45. Substituting this into the equilibrium expression, the ratio of cyclohexanol to phenol can be solved for as:



In a simple model reaction system, this would give a phenol selectivity of 74%. Though direct comparison of this model system to the HDO reaction studied is limited due to the number of products and reactions occurring, it is highly supportive that the formation of unsaturated species is thermodynamically favorable for similarly-structured oxygenates. Moreover, the obtained 2-hour selectivity towards PHE (4-propylphenol) over 0.4-Pt catalysts of 68% at low (14%) conversion aligns very well with the 74% estimated by this method. In the high (62%) conversion case, the agreement is lower at 42% selectivity to PHE, though this is likely impacted primarily by the favored formation of HYD from DHE, which prevents the formation of PHE and thus creates a significantly different system composition than estimated here via thermochemistry.

References

- [1] Kabo, G.J. *Thermodynamic properties of cyclohexanol and cyclohexanone*. **J. Chem. Thermodyn.** 1988, 20, 429-437.
- [2] Chase, M.W. Jr., *NIST-JANAF Thermochemical Tables, Fourth Edition*, **J. Phys. Chem. Ref. Data, Monograph 9**, 1998, 1-1951.
- [3] Wiberg, K.B., Wasserman, D.J., Martin, E.J., Murcko, M.A., *Enthalpies of hydration of alkenes. 3. Cycloalkenes*. **J. Am. Chem. Soc.**, 1985, 107, 6019-6022.
- [4] Cox, J.D. *The Heats of Combustion of Phenol and Three Cresols*. **Pure Appl. Chem.**, 1961, 2, 125-128.
- [5] Sarin, V.N., Jain, Y.S., Bist, H.D. *Thermodynamic Properties in the Gaseous State of Certain Monosubstituted Benzenes*. **Thermo. Acta**, 1973, 6, 39-46.